AMERICAN SOCIETY FOR MICROBIOLOGY | Infection and Immunity®

Yersinia pestis YopK Inhibits Bacterial Adhesion to Host Cells by Binding to the Extracellular Matrix Adaptor Protein Matrilin-2

Yafang Tan,[a] Wanbing Liu,[a] Qingwen Zhang,[b] Shiyang Cao,[a] Haihong Zhao,[b] Tong Wang,[a] Zhizhen Qi,[b] Yanping Han,[a] (ID) Yajun Song,[a] Xiaoyi Wang,[a] Ruifu Yang,[a] Zongmin Du[a]

State Key Laboratory of Pathogen and Biosecurity, Beijing Institute of Microbiology and Epidemiology, Beijing, China[a]; Key Laboratory for Plague Prevention and Control of Qinghai Province 2017-ZJ-Y15, Institute for Endemic Disease Prevention and Control of Qinghai Province, Xining, China[b]

ABSTRACT Pathogenic yersiniae harbor a type III secretion system (T3SS) that injects *Yersinia* outer protein (Yop) into host cells. YopK has been shown to control Yop translocation and prevent inflammasome recognition of the T3SS by the innate immune system. Here, we demonstrate that YopK inhibits bacterial adherence to host cells by binding to the extracellular matrix adaptor protein matrilin-2 (MATN2). YopK binds to MATN2, and deleting amino acids 91 to 124 disrupts binding of YopK to MATN2. A *yopK* null mutant exhibits a hyperadhesive phenotype, which could be responsible for the established Yop hypertranslocation phenotype of *yopK* mutants. Expression of YopK, but not YopK$_{\Delta 91-124}$, in a *yopK* mutant restored the wild-type phenotypes of adhesion and Yop translocation, suggesting that binding to MATN2 might be essential for YopK to inhibit bacterial adhesion and negatively regulate Yop translocation. A green fluorescent protein (GFP)-YopK fusion specifically binds to the endogenous MATN2 on the surface of HeLa cells, whereas GFP-YopK$_{\Delta 91-124}$ cannot. Addition of purified YopK protein during infection decreased adhesion of *Y. pestis* to HeLa cells, while YopK$_{\Delta 91-124}$ protein showed no effect. Taking these results together, we propose a model that the T3SS-secreted YopK hinders bacterial adhesion to HeLa cells by binding to MATN2, which is ubiquitously exposed on eukaryotic cells.

KEYWORDS *Yersinia pestis*, type III secretion, YopK, adhesion, MATN2, Yop translocation, phagocytosis

Yersinia pestis is the causative agent of plague, which has been known as the notorious Black Death in history (1). This lethal pathogen utilizes a virulence mechanism called the type III secretion system (T3SS) to deliver Yop (*Yersinia* outer protein) virulence effectors into the host cytosol, where they hijack host cell signaling pathways to inhibit host defenses (2, 3). Three human-pathogenic *Yersinia* species, *Y. pestis*, *Y. enterocolitica*, and *Y. pseudotuberculosis*, share a pCD1/pYV1-encoded T3SS that is indispensable for full virulence of these pathogens (2). Yop effectors delivered by the T3SS include at least YopH, YopE, YopM, YopT, YpkA/YopO, YopJ/YopP, and YopK/YopQ. A large number of studies have elucidated functions of those effectors and their contributions to pathogenesis (4–7). However, despite significant progress in recent years, our understanding on the role of YopK in *Yersinia* pathogenesis remains unclear (8–12).

YopK is almost identical in three pathogenic *Yersinia* species, and the YopK homolog in *Y. enterocolitica* is called YopQ. Evidence shows that YopK is a virulence factor for

pathogenic *Yersinia* (11, 13, 14). YopK has been shown to be essential for the full virulence of nonpigmented *Y. pestis* KIM in BALB/c mice via intravenous (i.v.) challenges (13). A *yopK* mutant of *Y. pseudotuberculosis* exhibited more than 40-fold virulence attenuation in intraperitoneally (i.p.) infected mice and also was attenuated in an oral infection (11). YopK was shown to be involved in control of Yop translocation across the eukaryotic cell membrane, and a *yopK* mutant delivered more Yop effectors into host cytosol, thereby inducing more rapid cytotoxic effects than the wild-type strain (12). Using a β-lactamase reporter assay, researchers demonstrated that YopK controls the rate and fidelity of Yop injection into host cytosol (9, 10). Dewoody et al. further confirmed that YopE and YopK act at different steps to control Yop translocation and that YopK acts independently of YopE to control Yop translocation from within host cells (9). Brodsky et al. proved that YopK interacts with the YopB/D translocon and prevents host inflammasome recognition of the *Yersinia* T3SS via an unknown mechanism, thereby leading to an inhibition of NLRP3 inflammasome activation (8). Thorslund et al. found that YopK interacts with the receptor for activated C kinase (RACK1) and that this interaction promotes the phagocytosis resistance of *Y. pseudotuberculosis* (15).

Our previous yeast two-hybrid screening experiment identified human extracellular matrix (ECM) adaptor protein matrilin-2 (MATN2) as an interacting partner of YopK (16). MATN2 is a widely distributed ECM component that interacts with ECM molecules, such as fibrillin 1, fibrillin 2, laminin, fibronectin, and different types of collagen (17), and it has been shown to be important in formation of collagen-dependent and -independent filamentous networks (18). In this study, we showed that YopK binds to the cell surface-exposed endogenous MATN2 and that purified YopK protein strongly inhibits the bacterial adherence to HeLa cells. A *yopK* null mutant exhibits hyperadhesive and Yop hypertranslocation phenotypes, and binding to MATN2 is essential for YopK to inhibit bacterial adhesion and negatively regulate Yop translocation, because deleting amino acids 91 to 124 of YopK results in loss of those functions.

RESULTS

Identification of amino acids essential for binding of YopK to MATN2. MATN2 was identified as an interacting protein of YopK in our previous yeast two-hybrid screening (16), and the matched mRNA corresponds to the C terminus of MATN2 (GenBank accession number NM_002380.3). To define regions that mediate the binding of YopK to human MTAN2, plasmids expressing different glutathione *S*-transferase (GST)-tagged YopK truncations were constructed (Fig. 1A and B; Table 1). The FLAG-tagged C terminus of MATN2 (MATN2-C) was overexpressed in human embryonic kidney 293T (HEK293T) cells, and GST control, GST-YopK, or GST-tagged YopK truncations were expressed in *Escherichia coli*. GST pulldown assay results confirmed that YopK interacts with MATN2-C (Fig. 1C). YopK$_{1-60}$, an N-terminal truncation of YopK, completely lost the ability to bind MATN2-C; however, C-terminal truncations of YopK, YopK$_{61-182}$ and YopK$_{91-182}$, interacted with MATN2-C as well as the full-length YopK, suggesting that the C-terminal amino acids 91 to 182 are sufficient for the binding of YopK to MATN2, whereas the N terminus is dispensable for the binding. YopK$_{1-124}$ retained a weak yet distinguishable affinity for MATN2-C, indicating that amino acids 61 to 124 of YopK are involved in, but are not sufficient for, MATN2 binding (Fig. 1C). We attempted to express YopK$_{125-182}$, but no expression could be detected, even though DNA sequencing revealed that the cloned sequence was correct. Thus, we could not determine whether this deletion mutant could bind to MATN2. Based on the above results, we constructed a plasmid expressing YopK lacking amino acids 91 to 124, which was then expressed in *E. coli* to determine whether this region is essential for MATN2 binding. GST pulldown results clearly demonstrated that YopK$_{\Delta91-124}$ did not bind to MATN2. We speculate that residues 125 to 182 of YopK might be important but insufficient for mediating this interaction, because YopK$_{91-182}$ interacted with MATN2-C, whereas YopK$_{\Delta91-124}$, which contains residues 125 to 182, did not. Similarly, residues 91 to 124 are also essential but insufficient for binding, since YopK$_{1-124}$
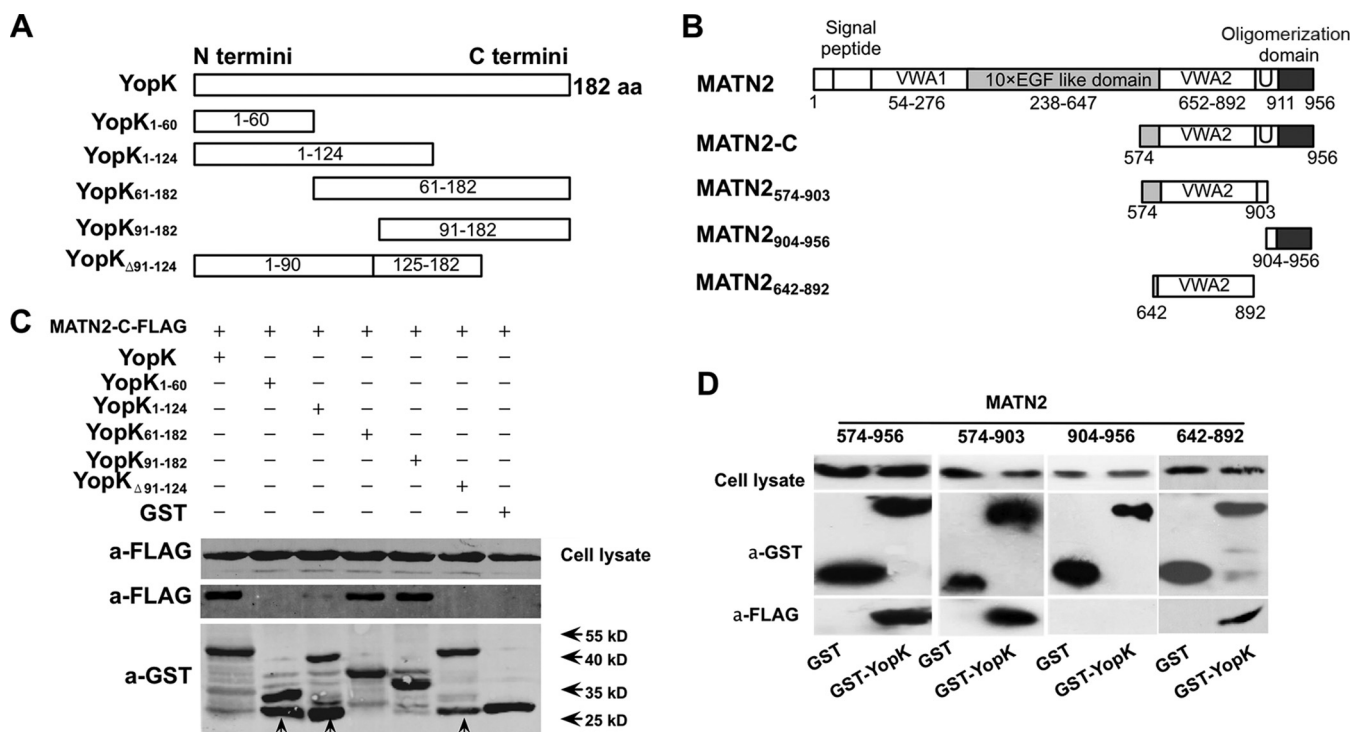
FIG 1 Amino acid residues 91 to 124 of YopK are critical for MATN2 binding. (A) Schematic diagrams of various YopK truncations. (B) Schematic diagrams of human MATN2 truncations. (C) A GST pulldown assay was used to identify the amino acids that are critical for the binding of YopK to MATN2. Arrows indicate the bands of degradation products or protein impurities. (D) Binding between GST-YopK and the MATN2 truncations was analyzed by GST pulldown assay. GST-tagged YopK or YopK truncations expressed in *E. coli* were bound to glutathione-Sepharose 4B beads. HEK293T cells were transfected with plasmids expressing MATN2 truncations. After 48 h of transfection, cells were lysed and stored at −80°C until use. Sepharose 4B beads bound with purified GST-tagged YopK or YopK truncations were incubated with cell lysates containing MATN2 or its truncations. The beads were thoroughly washed to remove the unbound proteins. Bound proteins were then eluted by boiling in sample buffer and separated by SDS-PAGE. Proteins were transferred onto a PVDF membrane and analyzed by immunoblotting using anti-FLAG or anti-GST antibodies.

showed merely a weak binding affinity for MATN2-C. Taken together, our results indicate that the C terminus of YopK (amino acids 91 to 128) mediates the binding to MATN2 and that the deletion of residues 91 to 124 disrupts this binding.

MATN2 contains an N-terminal signal peptide, two von Willebrand factor A (VWA) domains separated by 10 epidermal growth factor (EGF)-like motifs, and a C-terminal coiled-coil oligomerization domain that mediates homotetramer formation (17). To identify the regions that are essential for binding YopK, different MATN2 truncations were expressed and examined for their YopK binding affinity (Fig. 1D). All the truncations containing VWA2 domains were successfully pulled down by GST-YopK, suggesting that the VWA2 domain is sufficient for YopK binding and both the EGF-like domain and the oligomerization domain are dispensable. VWA domains are often involved in protein-protein interactions (17, 18), and a metal ion-dependent adhesion site (MIDAS) motif (DXSXSXnTXnD) in the VWA2 domain is thought to be involved in ligand binding. Thus, three point mutations D→A, T→A, and DSS→AAA, in the MIDAS of MATN2-C were expressed and analyzed for their binding affinity to YopK, but none of the mutations exhibited any defects in binding (see Fig. S1 in the supplemental material). These results demonstrate that the VWA2 domain mediates the binding of MATN2 to YopK in a manner independent of the MIDAS motif.

Taken together, our results indicate that YopK binds to MATN2 via the C-terminal residues 91 to 182. Deleting amino acids 91 to 124 of YopK disrupts MATN2 binding while keeping the N-terminal T3SS secretion signal intact; therefore, we used a *Y. pestis* strain expressing YopK$_{\Delta 91-124}$ to perform phenotype analysis in the following experiments.

Abundant YopK is present in the culture medium during HeLa cell infections. MATN2 is an ECM adaptor protein that functions primarily in the extracellular com-

TABLE 1 Bacterial strains and plasmids used in this study

Strain or plasmid	Relevant properties	Reference or source
Yersinia pestis strains		
201	Wild-type strain	48
201 Δ*yopK*	*yopK* gene of strain 201 replaced by a kanamycin cassette using the λRed recombinant system	This study
201 Δ*yopK*-C*yopK*	pACYC-*yopK* electroporated into 201 Δ*yopK*	This study
201 Δ*yopK*-C*yopK*$_{\Delta91-124}$	pACYC-*yopK*$_{\Delta91-124}$ electroporated into 201 Δ*yopK*	This study
201/YopE-TEM	pBBR1-YopE-TEM electroporated into 201	This study
201/YopK-TEM	pBBR1-YopK-TEM electroporated into 201	This study
201/TEM	pBBR1-TEM electroporated into 201	This study
201 Δ*yopK*/YopE-TEM	pBBR1-YopE-TEM electroporated into 201 Δ*yopK*	This study
201 Δ*yopK*-C*yopK*/YopE-TEM	pBBR1-YopE-TEM electroporated into 201 Δ*yopK*-C*yopK*	This study
Δ*yopK*-C*yopK*$_{\Delta91-124}$/YopE-TEM	pBBR1-YopE-TEM electroporated into 201 Δ*yopK*-C*yopK*$_{\Delta91-124}$	This study
Plasmids		
pET-YopK-GFP	*yopK* gene fused with GFP-coding sequence and cloned into pET28a	This study
pET-YopK$_{\Delta91-124}$-GFP	*yopK* gene lacking coding sequence of amino acids 91–124 fused to GFP gene and cloned into pET-28a	This study
pGEX-YopK	*yopK* gene cloned into pGEX-4T-2	This study
pGEX-YopK$_{1-60}$	Coding sequence of amino acids 1–60 of YopK cloned into pGEX-4T-2	This study
pGEX-YopK$_{1-124}$	Coding sequence of amino acids 1–124 of YopK cloned into pGEX-4T-2	This study
pGEX-YopK$_{61-124}$	Coding sequence of amino acids 61–124 of YopK cloned into pGEX-4T-2	This study
pGEX-YopK$_{91-182}$	Coding sequence of amino acids 91–124 of YopK cloned into pGEX-4T-2	This study
pGEX-YopK$_{\Delta91-124}$	*yopK* gene lacking coding sequence of amino acids 91–124 cloned into pGEX-4T-2	This study
pACYC-*yopK*	Coding sequence of *yopK* with ~300 bp of upstream sequence cloned into pACYC184	This study
pACYC-*yopK*$_{\Delta91-124}$	Coding sequence of *yopK* lacking bp 271–372 and ~300 bp of upstream sequence cloned into to pACYC184	This study
pBBR1MCS	Empty vector for construction of TEM-1 beta-lactamase reporter	Lab collection
pBBR1-TEM	TEM-1 beta-lactamase-coding sequence cloned into pBBR1MCS vector	This study
pBBR1-YopE-TEM	Coding sequence and ~300 bp upstream sequence of *yopE* cloned into pBBR1-TEM directly upstream of TEM-1-coding sequence	This study
pBBR1-YopK-TEM	Coding sequence and ~300 bp upstream sequence of *yopK* cloned into pBBR1-TEM directly upstream of TEM-1-coding sequence	This study

partment (17, 18). To address the biological significance of the interaction between YopK and MATN2, we first wanted to determine the cellular localization of YopK during infection. We used two approaches to do so.

The first method used immunoblotting for measurement of YopK in different cell fractions of the infected HeLa cells. First, we constructed a *Y. pestis yopK* mutant and the corresponding complemented strain. Bacterial strains were cultured in TMH medium (with or without calcium as indicated in Fig. 2A) at 37°C, and YopK expression and secretion into the culture medium were analyzed by immunoblotting. As expected, the Δ*yopK* strain did not produce or secret YopK under T3SS secretion-inducing conditions (without Ca²⁺ at 37°C), whereas the *yopK* mutant *trans*-complemented with *yopK*, (Δ*yopK*-C*yopK*) restored this ability, indicating that the *yopK* mutant and the *trans*-complemented strain were successfully constructed (Fig. 2A). HeLa cells were then infected with the wild-type, Δ*yopK*, or Δ*yopK*-C*yopK* strain for 2 h, and proteins from the cell culture medium, as well as the soluble and insoluble fractions of the infected HeLa cells, were analyzed for the presence of YopK using a YopK-specific polyclonal antibody. YopK was abundantly present in the culture medium but could not be detected in the soluble fraction of the cell lysates, although a large amount of YopK was found in the pellets containing cell debris and bacteria (Fig. 2B). A previous study showed that YopK could bind the YopB/D translocators (15). It was possible that some of the YopK molecules localized in the HeLa cell membranes by forming complexes with YopB/YopD. In contrast, YopM, an effector that has been shown to be translocated into eukaryotic cells (19), was abundantly present in both the soluble and insoluble fractions of the cell lysates (Fig. 2B), indicating that our system was capable of detecting Yops in the soluble fraction. These results demonstrate that in comparison to *bona fide* Yops such as YopM, YopK tends to be secreted into the extracellular compartment instead of the host cytosol.
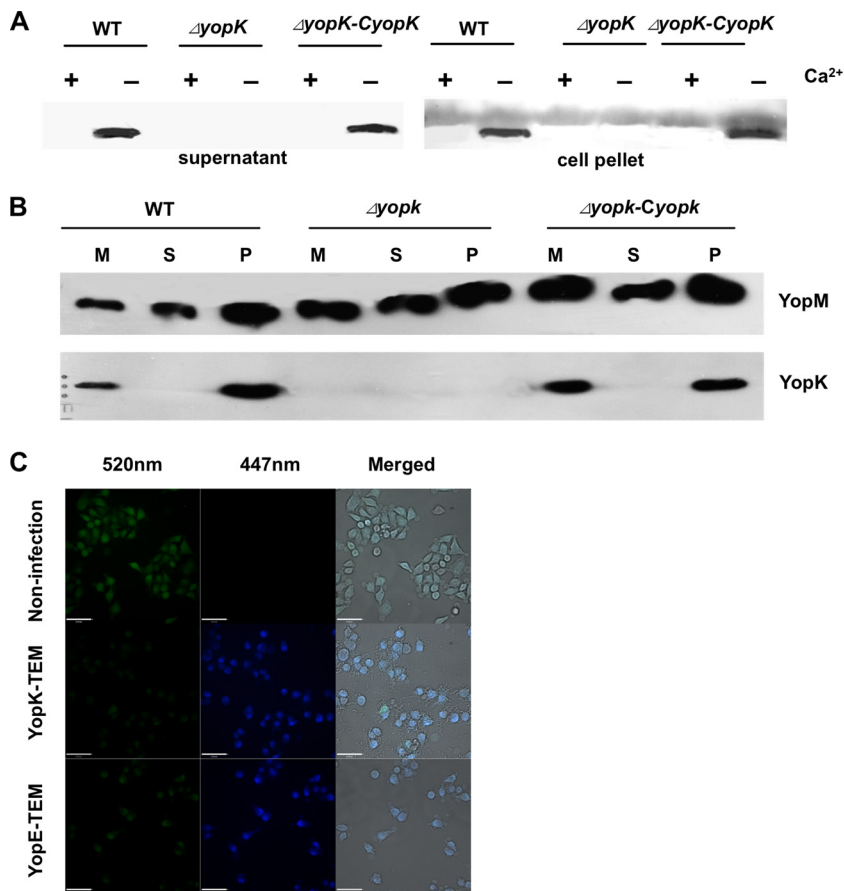
FIG 2 YopK secreted by *Y. pestis* is abundantly present in culture medium of infected HeLa cells. (A) Expression and secretion of YopK by different *Y. pestis* strains were analyzed by immunoblotting using anti-YopK antibody. The wild-type, ΔyopK, and ΔyopK-CyopK *Y. pestis* strains were cultured in TMH medium at 37°C with or without calcium as indicated. Secreted proteins in the culture supernatant and bacterial cell pellets were separated by SDS-PAGE and analyzed by immunoblotting using anti-YopK antibody. (B) Translocation of YopK into HeLa cells was analyzed by immunoblot detection of cell fractions using anti-YopK antibody. HeLa cells were infected with the indicated strains, and the culture medium (M) was collected after 2 h of infection. The infected cells were then lysed in 0.1% Triton X-100 and centrifuged to separate the supernatants (S) and cell pellets (P). Proteins in different cell fractions were separated by SDS-PAGE and immunoblotting using anti-YopK antibody. At least three independent experiments were performed, and a representative result is shown. (C) Translocation of YopK into HeLa cells was analyzed using a BlaTEM reporter. HeLa cells were infected with *Y. pestis* strains harboring pBBR1-*yopE*-TEM or pBBR1-*yopK*-TEM for 1 h. Cells were then loaded with 1 μg ml⁻¹ CCF2-AM substrate solution. Cell images were taken using an UltraVIEW Vox live-cell imaging system with an emission wavelength of 409 nm and detection wavelengths of 447 and 520 nm. All the scale bars represent 62 μm.

The second method used the β-lactamase reporter system reported by Marketon et al. (20). The lipophilic substrate CCF2-AM readily enters eukaryotic cells, and cleavage by endogenous cytoplasmic esterases rapidly converts CCF2-AM into CCF2, which consists of a cephalosporin core linking a 7-hydroxycoumarin to a fluorescein. Translocation of YopK fused with a β-lactamase reporter introduces β-lactamase into host cytosol, and enzymatic cleavages of CCF2 by β-lactamase spatially separates the two dyes and disrupts fluorescence resonance energy transfer (FRET), leading to an increased ratio of blue to green fluorescence (447/520 nm) with excitation at 409 nm. Both YopE and YopK could be translocated into HeLa cells (Fig. 2C), since very faint green but strong blue fluorescence (FRET disrupted) was detected (Fig. 2C, lower two panels). In contrast, no blue fluorescence could be detected in the uninfected control cells.

Given that the enzymatic activity-based β-lactamase reporter assay is much more sensitive than analysis of the cellular fractions by immunoblotting, we conclude that
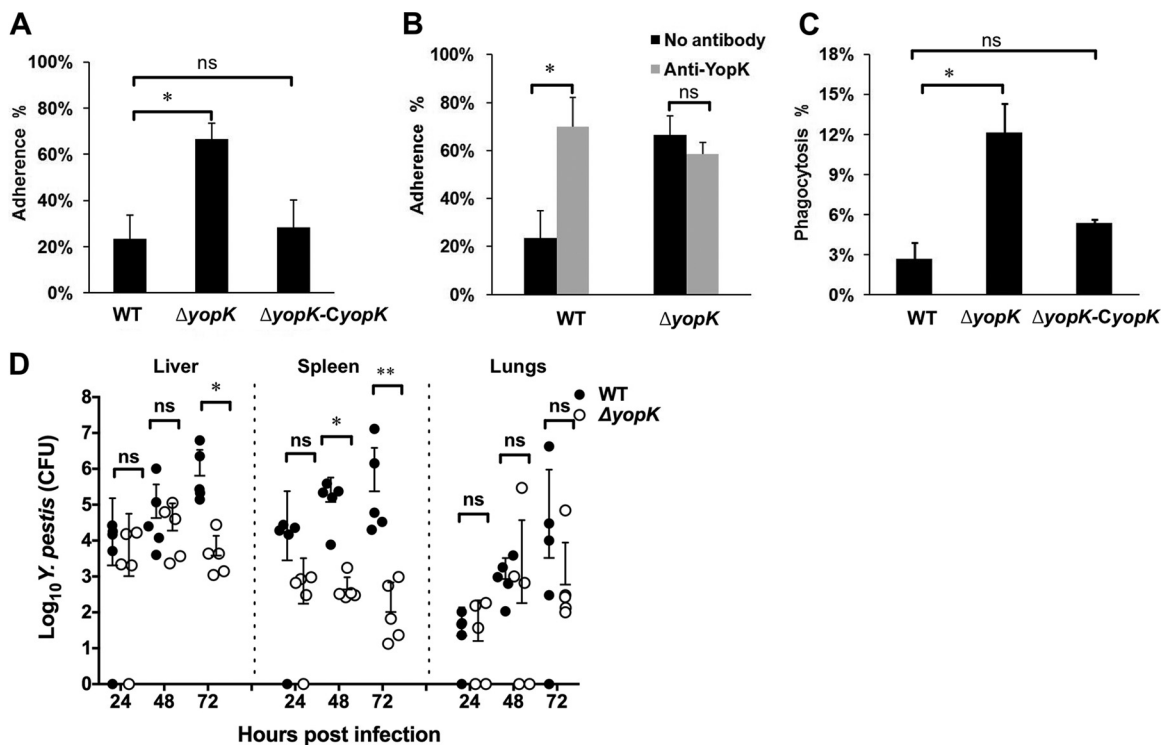
FIG 3 YopK inhibits bacterial adhesion to host cells and promotes resistance to phagocytosis by RAW264.7 cells. (A) HeLa cells were infected with the wild-type, ΔyopK, or ΔyopK-CyopK Y. pestis strain at an MOI of 100, and 1 μM cytochalasin D was added to inhibit the endocytosis of HeLa cells. After 2 h of infection, cells were extensively washed in prewarmed PBS to remove unattached bacteria and then lysed in 0.1% Triton X-100. The number of bacteria that adhered to the HeLa cells was counted by plating cell lysate dilutions on agar plates. The percentage of adhesion was calculated by dividing the number of attached bacteria by the total number of bacteria in the well. (B) HeLa cells were infected with the wild-type or ΔyopK Y. pestis strain as described for panel A except that anti-YopK antibody at 100 μg ml⁻¹ was present in the culture medium. The percentage of adhesion was calculated as described above. (C) RAW264.7 cells were infected with the indicated Y. pestis strains at an MOI of 20, and gentamicin was added into the culture medium after 0.5 h to kill the extracellular bacteria. Phagocytosed bacterial cells were counted by plating the diluted RAW264.7 cell lysates as described for panel A. All experiments were independently performed at least three times in triplicate. Statistical analysis was performed with GraphPad Prism version 6.0c for Mac using one-way ANOVA with Dunnett's multiple-comparison tests to analyze the significance of differences in bacterial adhesion or phagocytosis between the different strains. (D) Groups of mice (n = 5 for each group) were infected with ~100 CFU of wild-type or ΔyopK Y. pestis via i.v. injection. Mice were sacrificed at the indicated times, and the tissues were homogenized. The bacterial loads were measured by plating dilutions of homogenates on agar plates. Colonization of the ΔyopK mutant in spleen was greatly hampered at 48 and 72 hpi. In liver, the difference was significant only at 72 h. The significance of the differences between the mice infected with the wild-type and ΔyopK strains was determined by multiple t tests (**, $P < 0.01$; *, $P < 0.05$; ns, not significant).

YopK is abundantly present in the culture medium and that a relatively small portion is delivered into the cytosol of HeLa cells, probably because YopK binds to the host membrane-embedded YopB/D translocators or other membrane structures (15). Distribution of YopK during infection of a mammalian host needs further exploration, and this can be challenging because of the lack of an appropriate method to measure the extracellular Yops in vivo.

YopK inhibits bacterial adhesion to HeLa cells and promotes phagocytosis resistance to RAW264.7 macrophages. Because YopK is abundantly present in the culture medium during HeLa cell infections, we sought to determine whether YopK influences the adhesion of Y. pestis to host cells. Prior to infection, cytochalasin D was added to the cell cultures to inhibit endocytosis. HeLa cells were infected with the wild-type, ΔyopK, or ΔyopK-CyopK strain, and bacteria that were not associated with HeLa cells were removed by extensive washing. HeLa cells were lysed, and numbers of the liberated bacteria were determined by plating serial dilutions of the cell lysates onto agar plates. The ΔyopK strain exhibited a much higher level of adhesion to the HeLa cells than the wild-type strain, and the ΔyopK-CyopK strain restored the wild-type level of adhesion (Fig. 3A). We further analyzed the adhesion of different Y. pestis strains to HeLa cells after YopK was neutralized with a polyclonal antibody. Addition of a

TABLE 2 Virulence of the Δ*yopK* mutant in BALB/c mice determined via i.v. and s.c. challenges

| | LD$_{50}$ (CFU) after challenge: | | |
| | i.v. | | |
Y. pestis strain	First	Second	s.c.
201	94	31	6
201 Δ*yopK*	1,778	1,380	10
201 Δ*yopK*-C*yopK*	73	89	8.9

purified rabbit anti-YopK antibody to cell cultures significantly enhanced adhesion of the wild-type *Y. pestis* to HeLa cells but had no obvious impact on the Δ*yopK* strain (Fig. 3B). These data strongly indicate that YopK in the culture medium impedes the adhesion between *Y. pestis* and host cells and that an anti-YopK antibody can neutralize this impediment.

We further examined the antiphagocytic ability of the Δ*yopK* strain using RAW264.7 macrophages, since adhesion and phagocytosis are intimately related biological events during bacterial infections. Gentamicin was added to the culture medium after 0.5 h of infection to kill extracellular bacteria, and the numbers of engulfed bacteria were determined by plating serial dilutions of cell lysates onto agar plates. Compared to the wild-type strain, a much higher percentage of the Δ*yopK* bacteria were phagocytosed by RAW264.7 macrophages, while the Δ*yopK*-C*yopK* strain showed a phagocytosis resistance similar to that of the wild-type strain (Fig. 3C). The Δ*yopK* strain reproducibly exhibits a significantly lower phagocytosis resistance to RAW264.7 macrophages in repeated experiments. This result seems to be puzzling, because previous studies reported that the *yopK* mutant delivered more Yop effectors into host cytosol, including YopE, YpkA, and YopT, which target the host cytoskeleton to inhibit phagocytosis (12). We speculate that YopK deletion promotes bacterial adhesion to host cells, rendering the membrane receptors that recognize invading bacteria more accessible to the Δ*yopK* bacteria, which promotes bacterial recognition and phagocytosis. Taken together, these data demonstrate that the Δ*yopK* strain exhibits a lower phagocytosis resistance to macrophages, probably due to the absence of YopK in the culture medium greatly relieving the inhibitory effects of YopK on bacterial adhesion to host cells.

The *yopK* mutant of *Y. pestis* is highly attenuated in i.v. infected but not s.c. infected mice. In order to investigate the role of YopK in virulence of *Y. pestis* strain 201, we determined the 50% lethal dose (LD$_{50}$) of the Δ*yopK* mutant in i.v. or subcutaneously (s.c.) infected mice. Five groups of female BALB/c mice (*n* = 6 per group) were i.v. challenged via caudal vein or s.c. challenged at the inguina with different doses of each strain. The LD$_{50}$s of the Δ*yopK* mutant were shown to be 20- to 40-fold higher than those of the wild-type strain when inoculated by the i.v. route; however, no virulence attenuation was observed in the s.c. infected mice (Table 2). To monitor the colonization dynamics of mice infected with the *yopK* mutant, bacterial loads in lungs, liver, and spleen were determined in i.v. infected mice. No significant differences in lung or liver colonization could be observed between the wild-type- and Δ*yopK* mutant-infected mice at 24 or 48 h postinfection (hpi), and the differences in liver colonization became significant only at 72 hpi. In contrast, spleen colonization by the Δ*yopK* mutant was greatly impaired, and significant differences could be detected at 48 and 72 hpi (Fig. 3D). Attenuation of Δ*yopK* virulence in i.v. infected mice demonstrated that YopK is essential for the pathogenesis of *Y. pestis* strain 201, and our observation that the *yopK* mutant can barely colonize spleen is in line with the previous reports (8, 11).

***Y. pestis* expressing YopK$_{\Delta 91-124}$, which cannot bind to MATN2, exhibits hyperadhesive and Yop hypertranslocation phenotypes.** Knowing that deletion of *yopK* increases adhesion of *Y. pestis* to HeLa cells and that amino acids 91 to 124 of YopK are essential for binding to MATN2, we wondered whether binding of YopK to MATN2 is involved in the hyperadhesive phenotype of the Δ*yopK* strain. First, we
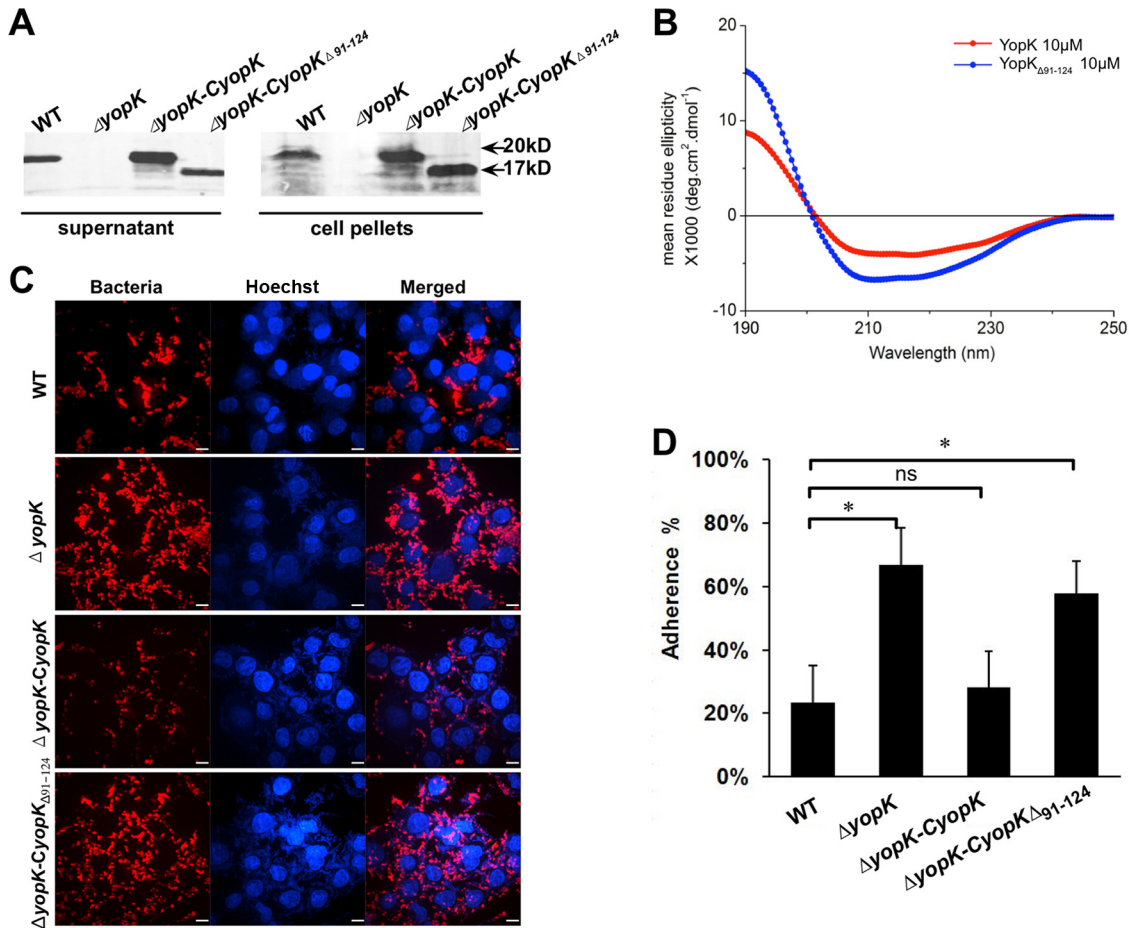
FIG 4 Expression of YopK$_{\Delta 91-124}$ in the $\Delta yopK$ strain does not restore a wild-type bacterial adhesion phenotype. (A) The *Y. pestis* strains were cultured in TMH medium without calcium at 37°C to an OD of 1.0. Bacterial cells and culture supernatants were collected by centrifugation, and the proteins were analyzed by SDS-PAGE and immunoblotting using anti-YopK antibody. YopK$_{\Delta 91-124}$ was secreted by $\Delta yopK$-C*yopK*$_{\Delta 91-124}$ at a level comparable to that of YopK secretion by the wild-type *Y. pestis*. (B) CD profiles in the far-UV range (190 to 250 nm) of YopK and YopK$_{\Delta 91-124}$ at 10 μM. The profiles represent the mean CD profiles for 8 measurements per protein. The buffer spectrum was subtracted from the proteins' spectra, and the resulting spectrum was analyzed with the online Dichroweb server. (C) HeLa cells were infected with the indicated strains at an MOI of 100 in the presence of 1 μM cytochalasin D. The percentage of adhesion was determined as described above. (D) HeLa cells were infected as described for panel C. After 2 h of infection, cells were extensively washed in prewarmed PBS to remove unattached bacteria, and the bacteria that adhered to HeLa cells were visualized using anti-F1 antigen monoclonal antibody and donkey anti-mouse IgG secondary antibody conjugated to Alexa Fluor 555. Scale bars in the images represent 9 μm. All experiments were independently performed at least three times in triplicate. Statistical analysis was performed using one-way ANOVA with Dunnett's multiple-comparison tests to analyze the significance of differences in bacterial adhesion between the different strains (*, $P < 0.05$; ns, not significant).

demonstrated that YopK$_{\Delta 91-124}$ could be secreted into the culture medium by the $\Delta yopK$-C*yopK*$_{\Delta 91-124}$ strain at a level comparable to that of YopK (Fig. 4A). This is consistent with the fact that *Yersinia* T3SS secretion signals are located at the N termini of Yops (21); therefore, deletion of amino acids 91 to 124 does not affect the secretion of YopK$_{\Delta 91-124}$. Secondary structures of YopK$_{\Delta 91-124}$ and YopK were assessed by the circular dichroism (CD) spectrum in far-UV spectra. The prediction of secondary structure was performed by the Dichroweb server (22, 23) and interpreted as a number of residues involved either in helices or strands, showing that the main change between YopK and YopK$_{\Delta 91-124}$ is the reduction in the number of residues involved in β-strands and turns. The results indicate that the deletion of residues 91 to 124 did not disrupt the overall protein conformation or result in protein aggregation (Fig. 4B). Adhesion of the wild-type, $\Delta yopK$, $\Delta yopK$-C*yopK*$_{\Delta 91-124}$, and $\Delta yopK$-C*yopK* strains to HeLa cells was analyzed as described above (Fig. 4C and D). Consistent with the results shown in Fig. 3A, adhesion of the $\Delta yopK$ strain to HeLa cells was significantly increased in comparison to that of the wild-type strain, and expression of the full-length YopK in a *yopK* null
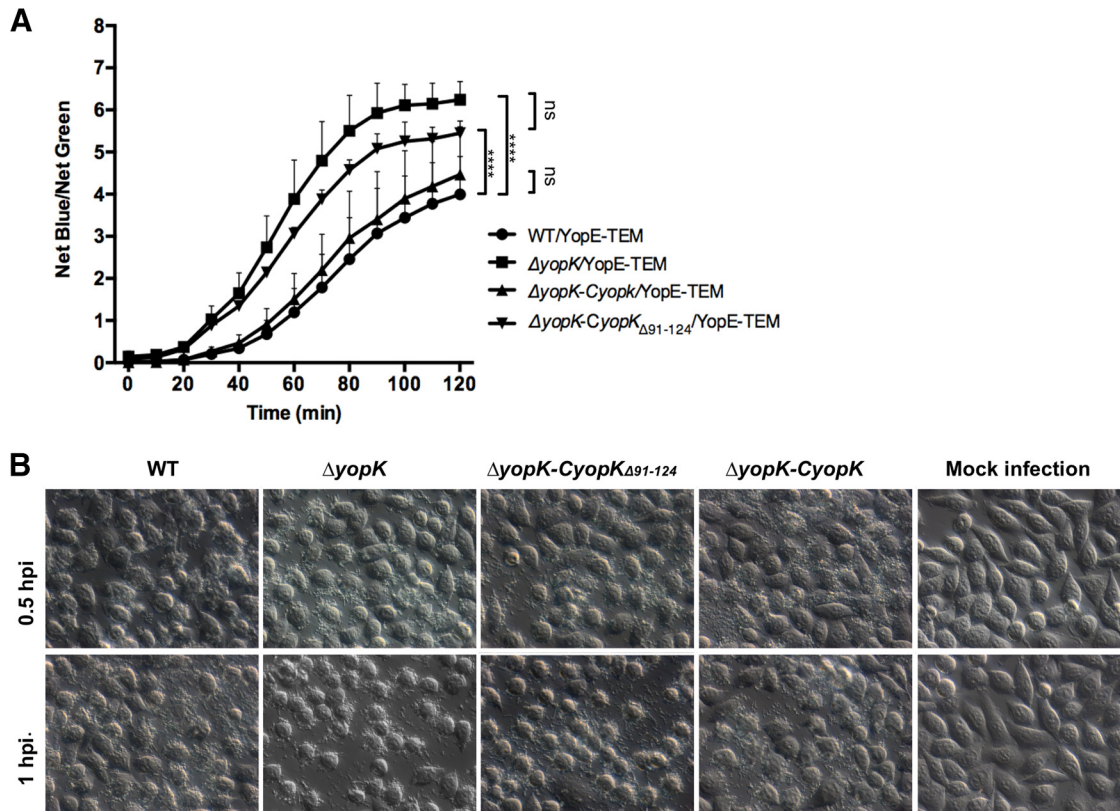
FIG 5 The Δ*yopK* strain expressing YopK$_{\Delta 91-124}$ exhibits Yop hypertranslocation. (A) The wild-type, Δ*yopK*, Δ*yopK*-C*yopK*, and Δ*yopK*-C*yopK*$_{\Delta 91-124}$ strains harboring plasmid pBBR1-*yopE*-TEM were used in this experiment, in which the expression of YopE fused with a C-terminal TEM is driven by the intrinsic *yopE* promoter. The strains were cultured at 26°C in BHI medium and shifted to 37°C for an additional 3 h of incubation for the full induction of the T3SS. HeLa cells at 70 to 80% confluence were infected with the aforementioned strains at an MOI of 20. After 1 h of infection, cells were loaded with 1 μg ml^{-1} CCF2-AM substrate solution, and the plates were incubated at 37°C and analyzed with SpectraMax M5. The means and standard deviations (SD) are indicated. ****, $P <$ 0.0001; ns, not significant (as determined by two-way ANOVA with Tukey's test for multiple pairwise comparisons). (B) HeLa cells were infected with different *Y. pestis* strains or mock infected as indicated. After 1 h of infection, DIC images of the infected cells were photographed under a Zeiss Axiovert 40 CFL microscope (Carl Zeiss, Germany).

mutant restored the wild-type adhesion phenotype. In contrast, a *yopK* mutant expressing YopK$_{\Delta 91-124}$, which cannot bind to MATN2, still showed the enhanced adhesion phenotype, suggesting that binding to MATN2 is essential for YopK to impede the adhesion between *Y. pestis* and host cells (Fig. 4D). Immunofluorescence detection of *Y. pestis* bacteria adhered to HeLa cells further confirmed these findings (Fig. 4C).

Previous studies have established that mutations of adhesins significantly impair Yop translocation into host cells (24, 25) and that mutation of *yopK* enhances Yop translocation (12). In order to test whether the inhibitory effect of YopK on bacterial adhesion to host cells is associated with the hypertranslocation phenotype, a TEM β-lactamase reporter plasmid expressing a YopE-TEM fusion protein was introduced into the wild-type, Δ*yopK*, Δ*yopK*-C*yopK*, and Δ*yopK*-C*yopK*$_{\Delta 91-124}$ strains, and the translocation of YopE-TEM into HeLa cells was analyzed. Consistent with previous reports (12), the *yopK* mutant translocated much more YopE-TEM fusion protein than the wild-type strain (Fig. 5A), and expression of full-length YopK, but not YopK$_{\Delta 91-124}$, which neither binds MATN2 nor inhibits the bacterial adhesion, in the Δ*yopK* strain restored the wild-type Yop translocation. In order to investigate whether the hypertranslocation of Yops will lead to a more rapid cytotoxic response, images of HeLa cells infected with the wild-type, Δ*yopK*, Δ*yopK*-C*yopK*, and Δ*yopK*-C*yopK*$_{\Delta 91-124}$ strains were taken using an inverted microscope at 0.5 and 1 hpi (Fig. 5B). As expected, almost all the HeLa cells infected with the Δ*yopK* and Δ*yopK*-C*yopK*$_{\Delta 91-124}$ strains rounded up significantly at 1 hpi, whereas a portion of cells infected with the wild-type strain did

not, demonstrating that the Δ*yopK* and Δ*yopK*-C*yopK*$_{\Delta91-124}$ strains exhibit higher cytotoxicity. Taken together, these data indicate that the inhibitory effect on bacterial adhesion requires amino acids 91 to 124 of YopK and that deletion of theses residues results in not only the hyperadhesive phenotype but also the Yop hypertranslocation phenotype.

Purified YopK protein inhibits the adhesion of *Y. pestis* to HeLa cells. Next, we want to analyze whether purified YopK can inhibit the adhesion of *Y. pestis* to host cells. The purified GST control, YopK, or YopK$_{\Delta91-124}$ protein was added to HeLa cell cultures, and the cells were infected with the wild-type or the Δ*yopK* strain. After 2 h of infection, the infected cells were thoroughly washed, and the percentages of adhesion of bacteria to HeLa cells were analyzed as described above. Similar to the results shown in Fig. 3, the Δ*yopK* strain consistently showed much higher adhesion to HeLa cells than the wild-type strain in multiple independent experiments (Fig. 6). Addition of purified YopK significantly reduced adhesion of both the wild-type and the *yopK* mutant strains. In contrast, addition of YopK$_{\Delta91-124}$ showed no obvious effect on adhesion of both strains. These data indicate that the purified YopK protein can inhibit the adhesion of *Y. pestis* to HeLa cells and that YopK$_{\Delta91-124}$, which cannot bind to MATN2, exhibits no inhibitory effect.

The purified GFP-YopK fusion specifically binds with the endogenous MATN2 on the HeLa cell surface. Next, we sought to determine whether YopK could interact with the endogenous MATN2 on the host cell surface. C-terminally GFP-tagged GST, YopK, or YopK$_{\Delta91-124}$ proteins were expressed in *E. coli*, and the corresponding purified GFP fusion proteins were incubated with HeLa cells overnight at 4°C. Endogenous MATN2 on the HeLa cell surface was visualized using an anti-MATN2 antibody, followed by staining with an Alexa Fluor 588-labeled secondary antibody. Purified GFP-YopK protein bound to HeLa cells, and the green fluorescent signals of GFP-YopK largely colocalized with MATN2, which was shown in red after visualization with the specific anti-MATN2 antibody and a red fluorescent secondary antibody (Fig. 7A). Only background green fluorescence similar to that of cells incubated with GFP-tagged GST was observed in HeLa cells incubated with purified GFP-YopK$_{\Delta91-124}$, and the colocalization signals were significantly decreased (Fig. 7A and B). SDS-PAGE analysis of the purified proteins confirmed that equal amounts of GFP-tagged YopK, YopK$_{\Delta91-124}$, or GST protein were added to the cultured HeLa cells (Fig. 7C). These data indicate that YopK could specifically colocalize with the endogenous MATN2 on HeLa cell surfaces.

DISCUSSION

YopK has been shown to be secreted by *Yersinia* bacteria into culture medium (11) but was not detected in the cytosol of infected cells using microscopy approaches (12). By using a novel reporter system that fused a phosphorylatable glycogen synthase kinase (GSK) tag to Yops, Garcia et al. detected the phosphorylation of the GSK tag during *Y. pestis* infection, demonstrating for the first time that YopK could be translocated into eukaryotic cells (26). Subsequently, two groups independently showed that YopK could be translocated into host cells by using a *β*-lactamase reporter assay (9, 15). Thorslund et al. (15) further showed that YopK interacts with the signaling protein RACK1, which binds to *β*1-integrins within the host cells. We used a cell fractionation analysis and a *β*-lactamase reporter assay to determine the localization of YopK during *Y. pestis* infection. While YopK was not detected in the soluble fraction of HeLa cell lysates, YopK-TEM translocation into HeLa cells was observed. Based on the reports from different groups, as well as our results of this study, we conclude that YopK is abundantly present in the extracellular compartment and that only a relatively small fraction of YopK is translocated to the host cytosol, probably because some of the YopK molecules bind to the YopB/YopD translocators or other membrane structures of host cells. The actual distribution of YopK in *Y. pestis*-infected mammalian hosts needs further investigation. The unique pattern of YopK localization during infection suggests that it might play a role in the extracellular compartment, for instance, by interacting with ECM proteins to promote infection.
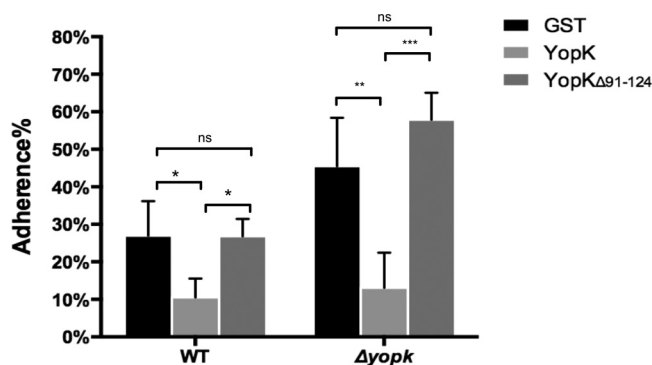
FIG 6 Purified YopK protein inhibits bacterial adhesion to HeLa cells. HeLa cells seeded in 12-well plates were grown to 80% confluence in the presence of 1 μM cytochalasin D. About 50 μg/ml of purified GST-YopK or GST-YopK$_{\Delta91-124}$ was added to the cell cultures, and then the cells were infected with the wild-type or $\Delta yopK$ *Y. pestis* strain at an MOI of 100. After 2 h of infection, cells were extensively washed in prewarmed PBS to remove the unattached bacteria and then lysed in 0.1% Triton X-100. The percentage of adhesion was determined as described for Fig. 3A. Addition of purified GST-YopK significantly lowered the adhesion of $\Delta yopK$ bacteria to HeLa cells, but addition of purified GST-YopK$_{\Delta91-124}$ exhibited no such effect. Two-way ANOVA with Bonferroni's multiple-comparison test was performed to analyze the significance of difference in bacterial adhesion between the different treatments (ns, not significant; *, $P < 0.05$; **, $P < 0.01$; ***, $P < 0.001$).

ECM proteins of eukaryotic cells constitute an important pathogen-host interface for their cross talk. Pathogenic yersiniae have evolved several adhesins that target ECM proteins during infections. YadA and Inv are two major outer membrane adhesins in enteropathogenic yersiniae (18, 27, 28) but are inactivated in *Y. pestis* (29–31), and both of them promote intimate bacterium-host cell contacts by binding to β-integrin receptors and other ECM proteins on the host cell membrane (31). Ail, an OmpX family member that binds to laminin, fibronectin, and negatively charged heparin sulfate proteoglycan (32, 33), is the major adhesin of *Y. pestis*. Psa forms fimbriae at the bacterial surface and promotes the adhesiveness and invasiveness of *Y. pestis* (34, 35). Distinct from enteropathogenic yersiniae, *Y. pestis* harbors an additional adhesin, named plasminogen activator (Pla), that is encoded by pPCP1plasmid and binds to laminin and host receptors (36, 37). All these adhesins are outer membrane proteins that are firmly embedded in the bacterial membrane. Despite the functional differences among these adhesins, defects in any of them impair the efficient translocation of Yops (25, 38).

YopK is obviously distinct in two main aspects from the aforementioned adhesins that bind to ECM proteins. First, YopK can be secreted by bacterial cells rather than anchored to bacterial membrane. Second, YopK inhibits, rather than promotes, bacterial adhesion to host cells. Although both these adhesins and YopK bind to ECM proteins on the host cell surface, the outcomes are completely different. Adhesins anchored on bacterial membranes tether bacteria to host cells, whereas free molecules of YopK impede the intimate bacterium-host cell contacts by binding to MATN2, an ECM protein ubiquitously expressed at the surface of eukaryotic cells. Our results explain why *pla*, *psa*, and *ail* mutations hamper Yop delivery (38), whereas a *yopK* mutation leads to a hypertranslocation phenotype (12).

It seems paradoxical that the *yopK* mutant exhibits hypertranslocation of Yops and higher cytotoxicity to HeLa cells (9, 12) but is attenuated in i.v. infected mice, as shown in our virulence assay as well as in previous studies (11, 13). We believe that these results demonstrate that successful systemic infection requires tightly regulated Yop translocation and adhesion to host cells. In addition, YopK has been shown to play multiple roles in *Yersinia* pathogenesis, from preventing innate immune recognition of the *Yersinia* T3SS to the RACK1 signaling pathway (8, 15), and thus the virulence attenuation of the $\Delta yopK$ mutant could be a comprehensive result caused by the loss of those established activities. It is remarkable that virulence attenuation was observed
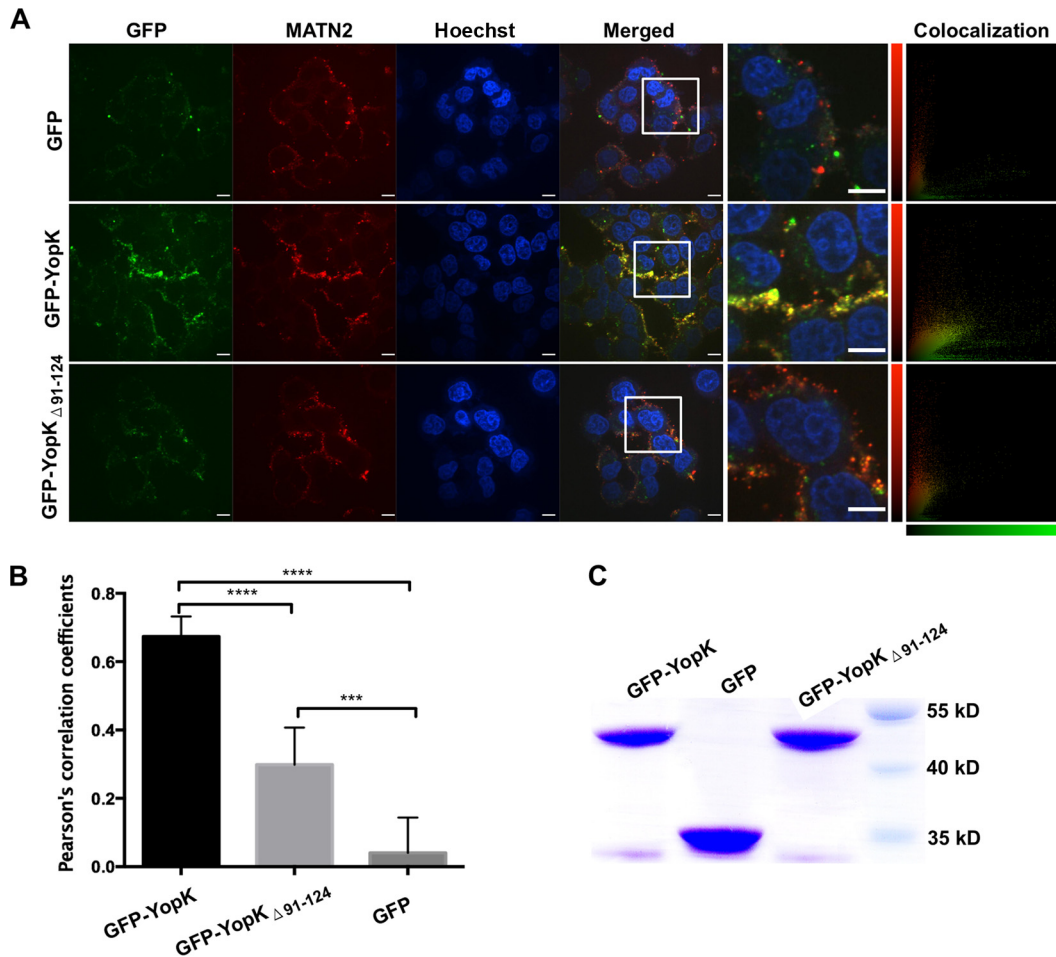
FIG 7 YopK colocalizes with the endogenous MATN2 on the HeLa cell surface. (A) Equal amounts of purified GFP-YopK, GFP-YopK$_{\Delta91-124}$, or GFP were added into HeLa cells and incubated at 4°C overnight. Endogenous MATN2 on the HeLa cell surface was visualized using a rabbit anti-MATN2 antibody and a donkey anti-rabbit IgG secondary antibody conjugated to Alexa Fluor 555. All scale bars represent 9 μm. Images were acquired using an UltraVIEW Vox live-cell imaging system, and Pearson's correlation coefficient was used to quantify the degree of colocalization between the two channels (red and green) in a confocal image by using Volocity 6.1 software. (B) The bar graphs were drawn to show average Pearson's correlation coefficients (with error bars) from multiple images ($n = 7$ for each treatment) of the HeLa cells incubated with different proteins. One-way ANOVA with Bonferroni's multiple-comparison test was performed to analyze the significance of difference in bacterial adhesion between the different treatments (***, $P < 0.001$; ****, $P < 0.0001$). (C) SDS-PAGE analysis of the purified proteins confirmed that equal amounts of GFP-tagged YopK, YopK$_{\Delta91-124}$, or GST protein were added to cell cultures.

only in i.v. infected mice and not in s.c. infected mice. Adhesion capability is crucial for a bacterial pathogen to colonize and disseminate within the host, and the hyperadhesive phenotype of the Δ*yopK* mutant might benefit systemic infection in s.c. infected mice, which compensates for disadvantages caused by lower phagocytosis resistance. However, the impaired phagocytosis resistance of the Δ*yopK* mutant is unfavorable for fighting against the blood professional phagocytic cells in i.v. infected mice, resulting in virulence attenuation in i.v. infection. Accordingly, the Δ*yopK* mutant cannot colonize spleen that contains abundant phagocytes, but colonization of lung and liver seems to be unaffected.

Y. pestis has evolved from its enteropathogenic progenitor *Y. pseudotuberculosis* (39). Inv and YadA are indispensable for colonization of Peyer's patches and the mesenteric lymph nodes by enteropathogenic yersiniae (40, 41) but are inactivated in *Y. pestis*. Introduction of a functional Inv or YadA protein into *Y. pestis* led to a significant virulence attenuation (42, 43), suggesting that these adhesins cause harmful effects for *Y. pestis* during evolution. Although the *yopK* gene was conserved among the three pathogenic *Yersinia* species, YopK was shown neither to have a role in phagocytosis

resistance nor to cause cytotoxicity in HeLa cells in *Y. pseudotuberculosis*, probably partially due to the tight adhesion mediated by Inv and YadA overwhelming the effect of YopK. However, it was shown to be required to cause a systemic infection in both i.p. and orally infected mice (11). The *yopK* mutant strain was able to colonize the Peyer's patches at a lower efficiency than the wild-type strain, whereas it was unable to colonize the spleen after oral administration, which is consistent with our finding that the Δ*yopK* mutant of the 201 strain is unable to colonize spleen.

Newly acquired flea-borne transmission profoundly influenced the pathogenesis of *Y. pestis*. The plague bacterium seems to be able to tightly regulate its adhesiveness and antiphagocytic ability during infection. Inactivation of the major adhesins, Inv and YadA, for the enteropathogenic *Yersinia* in *Y. pestis* strongly supports this point. Being highly adhesive at the initial stage of infection promotes *Y. pestis* invasion of macrophages, where it replicates in a safe niche, whereas being less adhesive at the later stage of infection helps it to escape from phagocytosis. The regulatory role of YopK in *Y. pestis* adhesion via binding to the ECM adaptor MTAN2 identifies a novel virulence mechanism of this pathogen and improves our understanding of the pathogenesis of *Y. pestis*.

MATERIALS AND METHODS

Bacterial strains and culture conditions. *Y. pestis* biovar Microtus strain 201 (44) was used in this study (Table 1). Wild-type *Y. pestis* and various mutant strains were grown in brain heart infusion (BHI) broth or chemically defined TMH medium. *E. coli* strains DH5α and DE3 were grown in Luria-Bertani (LB) broth. Appropriate antibiotics were added when culturing bacteria carrying drug resistance markers.

Cell cultures, transfection, and antibodies. HEK293T, HeLa, and RAW264.7 cells were maintained in Dulbecco's modified Eagle's medium (DMEM) or RPMI 1640 medium (HyClone, GE Healthcare, Little Chalfont, UK) containing 10% fetal bovine serum and 2 mM L-glutamine at 37°C in a 5% CO_2 incubator. HEK293T cells were transfected using MegaTran 1.0 (OriGene, Rockville, MD, USA) to express MATN2 truncations according to the manufacturer's instructions. Antibodies against the GST tag and MATN2 were purchased from Santa Cruz Biotechnology (Dallas, TX, USA). Antibodies against FLAG-M2 and actin, as well as a horseradish peroxidase (HRP)-labeled goat anti-rabbit secondary antibody, were purchased from Sigma-Aldrich (St. Louis, MO, USA). Alexa Fluor 555-conjugated donkey anti-rabbit IgG and anti-mouse IgG were purchased from Invitrogen (Carlsbad, CA, USA). Polyclonal antibodies against YopK or YopM were generated in rabbits as previously described (45).

DNA manipulations. (i) Constructs for pulldown assays. Different fragments of the *yopK* coding sequence were amplified by PCR using specific primers and cloned into the pGEX-4T-2 vector to express various truncations of YopK in *E. coli* (Table 1). The *yopK* coding sequence with a deletion of bp 271 to 372 was generated by fusion PCR. The *MTAN2* cDNA sequence and the different PCR-amplified *MATN2* fragments were cloned into the pFLAG-CMV vector to express MATN2 and its truncations in HEK293T cells.

(ii) Construction of the *yopK* mutant and the *trans*-complemented strains. The *yopK* mutant of *Y. pestis* was constructed using λRed-based homologous recombination. The kanamycin resistance cassette used for homologous recombination was amplified from pKD4 using the primer pair *yopK*-KF and *yopK*-KR (see Table S1 in the supplemental material), and the *yopK* mutant was constructed as previously described (46). For *trans*-complementation, a DNA fragment containing ~300 bp of upstream sequence and the full *yopK* coding sequence was amplified using *yopK*-CF and *yopK*-CR and then cloned into pACYC184. The ~300-bp upstream sequence of the *yopK* gene was amplified, fused with *yopK* coding sequence lacking bp 271 to 372, and then cloned into pACYC184. The recombinant plasmids pACYC184-*yopk* and pACYC184-*yopk*$_{\Delta 91-124}$ were electroporated into the Δ*yopK* strain to generate the Δ*yopK*-C*yopK* and Δ*yopK*-C*yopK*$_{\Delta 91-124}$ strains, respectively.

(iii) Constructs for the BlaTEM translocation assay. The *blaTEM-1* coding sequence was cloned into pBBR1MCS to generate pBBR1-TEM, and then ~300 bp of upstream sequence and the coding sequences of *yopE* and *yopK* were amplified and inserted directly upstream of the *blaTEM* gene in pBBR1-TEM, generating pBBR1-*yopE*-TEM and pBBR1-*yopK*-TEM reporters, respectively. The pBBR1-*yopE*-TEM plasmid was electroporated into the wild-type, Δ*yopK*, Δ*yopK*-C*yopK*, and Δ*yopK*-C*yopK*$_{\Delta 91-124}$ strains to obtain YopE-TEM reporter strains in various genetic backgrounds (Table 1).

Protein expression and purification. The coding sequences of *yopK* and *yopK*$_{\Delta 91-124}$ were cloned into pET28a, and the GFP gene amplified using pGEX-4T-2 as the template was fused to the 3' ends of the *yopK* and *yopK*$_{\Delta 91-124}$ coding sequences. Expression of YopK and YopK$_{\Delta 91-124}$ with an N-terminal His tag and a C-terminal GFP tag in *E. coli* was induced with 0.1 mM isopropyl-1-thio-β-D-galactopyranoside (IPTG) at 20°C for 12 h. Bacterial cells were harvested, suspended in phosphate-buffered saline (PBS), and lysed by sonication. Bacterial lysates were centrifuged for 20 min at 12,000 rpm to remove bacterial debris, and the soluble recombinant proteins were purified by affinity chromatography using Ni-nitrilotriacetic acid (NTA) agarose (Qiagen, Valencia, CA, USA).

GST pulldown analysis. Purified GST-tagged YopK and its truncations were bound to glutathione-Sepharose 4B beads. HEK293T cells were transfected with plasmids expressing MATN2 and its various truncations. After 2 days, the cells were harvested, washed with ice-cold PBS, and lysed in lysis buffer (20

mM Tris-HCl [pH 8.0], 180 mM NaCl, 0.5% NP-40, 1 mM EDTA) supplemented with a protease inhibitor complete cocktail (Roche, Basel, Switzerland). The cell lysates were clarified and incubated at 4°C overnight with glutathione-Sepharose 4B beads bound with either GST or GST-tagged proteins. The beads were washed extensively, and bound proteins were boiled in Laemmli buffer, separated by 8% sodium dodecyl sulfate-polyacrylamide gel electrophoresis (SDS-PAGE), and analyzed by immunoblotting with appropriate antibodies.

Cell adhesion and phagocytosis assays. For adhesion assays, HeLa cells were seeded into a 24-well plate at a concentration of 4×10^5 cells ml^{-1} the day before infection. Wild-type *Y. pestis* 201 and various mutants were grown at 26°C to an optical density at 600 nm (OD_{600}) of ~1.0 and then shifted to 37°C for 3 h to induce maximal T3SS expression. Bacterial cells were collected and resuspended in DMEM, and bacterial concentrations were determined by measuring the OD_{600}. Serial dilutions of the bacterial suspensions were plated onto agar plates to count the actual number of the bacteria. Cytochalasin D was added to HeLa cells at a 1 μM concentration 1 h prior to infection. HeLa cells were infected with bacterial strains at a multiplicity of infection (MOI) of 100 and then centrifuged for 5 min at $500 \times g$ to promote contact between bacteria and HeLa cells. After 2 h of infection, HeLa cells were thoroughly washed for 5 min using prewarmed PBS. Cell-associated bacteria were liberated by treatment with 0.1% Triton X-100 in sterile H_2O for 15 min. The number of cell-associated bacteria was divided by the total number of bacteria in a well to calculate the adhesion percentage. Experimental procedures were the same as in the adhesion assay described above except that purified GST-YopK or GST-YopK$_{\Delta 91-124}$ at 50 μg/ml was added to the culture medium in order to evaluate the effects of YopK or YopK$_{\Delta 91-124}$ protein on the bacterial adhesion. For the phagocytosis assay, RAW264.7 cells were seeded into a 24-well plate at a density of 5×10^5 cells ml^{-1} the day before infection. RAW264.7 cells were infected with various *Y. pestis* strains at an MOI of 20, and 200 ng ml^{-1} gentamicin was added 0.5 h later to kill the extracellular bacteria. After 2 h of infection, the infected RAW264.7 cells were washed thoroughly with warm PBS 3 times and then lysed in 0.1% Triton X-100 for 15 min. The number of intracellular bacteria was divided by the total number of bacteria in a well to calculate the phagocytosis percentage. Statistical analysis was performed with GraphPad Prism version 6.0c for Mac using one-way analysis of variance (ANOVA) with Dunnett's multiple-comparison tests to analyze the significance of differences in bacterial adhesion or phagocytosis between the different strains. Two-way ANOVA with Bonferroni's multiple-comparison test was used to analyze the significance of differences in bacterial adhesion between YopK and YopK$_{\Delta 91-124}$ treatments.

Determination of virulence and colonization of the bacterial strains in mice. *Y. pestis* strains were cultured in BHI, and the bacterial cells were washed and suspended in PBS. Serially 10-fold-diluted bacterial suspensions in PBS were plated in triplicate on agar plates and incubated at 26°C to determine the actual challenge dose. Five groups of female BALB/c mice ($n = 6$ per group) were i.v. challenged via the caudal vein or s.c. challenged at the inguina with different doses of bacteria. The 50% lethal dose (LD_{50}) values were determined by the method of Reed and Muench (47). For the dynamic colonization analysis of the different strains, 3 groups of animals ($n = 5$) were i.v. challenged via the caudal vein with the *Y. pestis* wild-type and Δ*yopK* strains. One group of infected mice were sacrificed at 12, 48, and 72 hpi, and the lungs, spleens, and livers were removed and homogenized. The numbers of bacteria in tissue homogenates were counted by plating serial dilutions on agar plates. All the animal infection experiments were carried out in accordance with the license of the Ministry of Health in the General Logistics Department of the Chinese People's Liberation Army, permit no. SCXK-2007-004. Statistical analysis was done using the GraphPad Prism software by two-way ANOVA followed by Dunnett's multiple-comparison tests.

Cytotoxicity assay. HeLa cells were seeded into 24-well plates and grown to 80% confluence. *Y. pestis* strains were grown in BHI at 26°C overnight, and the bacterial cells were harvested by centrifugation and resuspended in DMEM. HeLa cells were infected with *Y. pestis* strains at an MOI of 10. After 1 h of infection, differential interference contrast (DIC) images of the infected cells were photographed under a Zeiss Axiovert 40 CFL microscope (Carl Zeiss, Germany).

Western blot analysis of Yop translocation. HeLa cells were seeded into a 24-well plate, allowed to reach 80 to 90% confluence, and then infected with *Y. pestis* strains at an MOI of 10. After 2 h of infection, the culture medium was collected into prechilled tubes, and proteins in the culture medium were precipitated overnight with 10% trichloroacetic acid (TCA) in ice-water bath. Infected HeLa cells were washed once in PBS and lysed in 0.1% Triton X-100 in sterile H_2O for 15 min at room temperature (bacterial cells remain intact under this condition), and the cell lysates were centrifuged at 12,000 rpm for 30 min at 4°C to separate the supernatant and precipitates containing cell debris and bacterial cells. Proteins in the supernatants were TCA precipitated as described above. The precipitated proteins and the insoluble cell pellets were mixed with Laemmli loading buffer and separated by12% SDS-PAGE, followed by transfer onto a polyvinylidene fluoride (PVDF) membrane (GE Healthcare, Piscataway, NJ, USA). Specific proteins were detected using rabbit polyclonal antibodies against YopK and YopM and an HRP-labeled goat anti-rabbit secondary antibody.

TEM assay for Yop translocation. HeLa cells were seeded into 96-well plate with black walls and clear bottoms (Invitrogen, Carlsbad, CA, USA). When they reached 60 to 70% confluence, HeLa cells were infected with *Y. pestis* strains harboring the TEM reporter plasmids at an MOI of 10. After 1 h of infection, the culture medium of the infected cells was removed and replaced with fresh DMEM containing the CCF2-AM substrate according to the manufacturer's instructions (Invitrogen, Carlsbad, CA, USA). The plates were incubated at 37°C and analyzed by using SpectraMax M5 (Molecular Devices, Sunnyvale, CA, USA), or they were observed using an UltraVIEW Vox live-cell imaging system (PerkinElmer, Waltham, MA, USA) with an emission wavelength of 409 nm and detection wavelengths of 447 and 520 nm. Two-way

ANOVA with Tukey's test for multiple pairwise comparisons was performed using GraphPad Prism version 6.0c to analyze the significance of differences between the different strains.

CD. Circular dichroism (CD) spectra were recorded on a J-815 spectrophotometer (JASCO, Easton, MD, USA) in the far-UV range (190 to 250 nm). Purified GST-YopK and GST-YopK$_{\Delta 91-124}$ were analyzed at a concentration of 10 μM in 25 mM Tris-HCl (pH 8)–150 mM NaF. Spectra were recorded at 25°C in 1-mm quartz cells at a rate of 50 nm min^{-1} with a data interval of 0.5 nm. The mean of the eight acquisitions was calculated after the buffer spectrum was subtracted from the proteins' spectra, and the resulting spectrum was analyzed with the online Dichroweb server (http://dichroweb.cryst.bbk.ac.uk/html/home.shtml).

Immunofluorescence staining and confocal microscopy. HeLa cells were seeded into glass-bottom culture dishes (MatTek Corporation, Ashland, MA, USA) at a concentration of 4×10^5 cells ml^{-1} the day before the experiment. Purified GFP-YopK, GFP-YopK$_{\Delta 91-124}$, or GFP at 0.1 mg ml^{-1} was added to the HeLa cell cultures. After overnight incubation at 4°C, the culture medium was depleted and the cells were washed thoroughly. Endogenous MATN2 on the HeLa cell surface was visualized using a rabbit polyclonal antibody against MATN2 and Alexa Fluor 555-conjugated donkey anti-rabbit IgG. Images were acquired using an UltraVIEW Vox live-cell imaging system (PerkinElmer). Pearson's correlation coefficient was used to quantify the degree of colocalization between the two channels (red and green) in a confocal image by using Volocity 6.1 software. Statistical analysis was performed with GraphPad Prism version 6.0c for Mac using one-way ANOVA with Dunnett's multiple-comparison tests to analyze the significance of differences in colocalization between the different samples.

For adhesion assay by immunofluorescence detection, HeLa cells were infected with the bacterial strains at an MOI of 100. Bacteria that were not tightly associated with HeLa cells were thoroughly washed away, and the HeLa cells were fixed with 3.8% paraformaldehyde for 30 min. *Y. pestis* cells were visualized with a monoclonal antibody against the F1 antigen and Alexa Fluor 555-conjugated donkey anti-mouse IgG. Images were acquired using an UltraVIEW Vox live-cell imaging system.

SUPPLEMENTAL MATERIAL

Supplemental material for this article may be found at https://doi.org/10.1128/IAI.01069-16.

SUPPLEMENTAL FILE 1, PDF file, 0.5 MB.

ACKNOWLEDGMENTS

REFERENCES

1. Pucovsky V, Harhun MI, Povstyan OV, Gordienko DV, Moss RF, Bolton TB. 2007. Close relation of arterial ICC-like cells to the contractile phenotype of vascular smooth muscle cell. J Cell Mol Med 11:764–775. https://doi.org/10.1111/j.1582-4934.2007.00066.x.

2. Cornelis GR, Boland A, Boyd AP, Geuijen C, Iriarte M, Neyt C, Sory MP, Stainier I. 1998. The virulence plasmid of Yersinia, an antihost genome. Microbiol Mol Biol Rev 62:1315–1352.

3. Cornelis GR. 2002. Yersinia type III secretion: send in the effectors. J Cell Biol 158:401–408. https://doi.org/10.1083/jcb.200205077.

4. Black DS, Bliska JB. 1997. Identification of p130Cas as a substrate of Yersinia YopH (Yop51), a bacterial protein tyrosine phosphatase that translocates into mammalian cells and targets focal adhesions. EMBO J 16:2730–2744. https://doi.org/10.1093/emboj/16.10.2730.

5. Monack DM, Mecsas J, Ghori N, Falkow S. 1997. Yersinia signals macrophages to undergo apoptosis and YopJ is necessary for this cell death. Proc Natl Acad Sci U S A 94:10385–10390. https://doi.org/10.1073/pnas.94.19.10385.

6. McDonald C, Vacratsis PO, Bliska JB, Dixon JE. 2003. The yersinia virulence factor YopM forms a novel protein complex with two cellular kinases. J Biol Chem 278:18514–18523. https://doi.org/10.1074/jbc.M301226200.

7. Shao F, Vacratsis PO, Bao Z, Bowers KE, Fierke CA, Dixon JE. 2003. Biochemical characterization of the Yersinia YopT protease: cleavage site

and recognition elements in Rho GTPases. Proc Natl Acad Sci U S A 100:904–909. https://doi.org/10.1073/pnas.252770599.

8. Brodsky IE, Palm NW, Sadanand S, Ryndak MB, Sutterwala FS, Flavell RA, Bliska JB, Medzhitov R. 2010. A Yersinia effector protein promotes virulence by preventing inflammasome recognition of the type III secretion system. Cell Host Microbe 7:376–387. https://doi.org/10.1016/j.chom.2010.04.009.

9. Dewoody R, Merritt PM, Houppert AS, Marketon MM. 2011. YopK regulates the Yersinia pestis type III secretion system from within host cells. Mol Microbiol 79:1445–1461. https://doi.org/10.1111/j.1365-2958.2011.07534.x.

10. Spanier B, Starke M, Higel F, Scherer S, Fuchs TM. 2010. Yersinia enterocolitica infection and tcaA-dependent killing of Caenorhabditis elegans. Appl Environ Microbiol 76:6277–6285. https://doi.org/10.1128/AEM.01274-10.

11. Holmstrom A, Rosqvist R, Wolf-Watz H, Forsberg A. 1995. Virulence plasmid-encoded YopK is essential for Yersinia pseudotuberculosis to cause systemic infection in mice. Infect Immun 63:2269–2276.

12. Holmstrom A, Petterson J, Rosqvist R, Hakansson S, Tafazoli F, Fallman M, Magnusson KE, Wolf-Watz H, Forsberg A. 1997. YopK of Yersinia pseudotuberculosis controls translocation of Yop effectors across the eukaryotic cell membrane. Mol Microbiol 24:73–91. https://doi.org/10.1046/j.1365-2958.1997.3211681.x.

13. Straley SC, Cibull ML. 1989. Differential clearance and host-pathogen interactions of YopE⁻ and YopK⁻ YopL⁻ Yersinia pestis in BALB/c mice. Infect Immun 57:1200–1210.

14. Holmstrom A, Rosqvist R, Wolf-Watz H, Forsberg A. 1995. YopK, a novel virulence determinant of Yersinia pseudotuberculosis. Contrib Microbiol Immunol 13:239–243.

15. Thorslund SE, Edgren T, Pettersson J, Nordfelth R, Sellin ME, Ivanova E, Francis MS, Isaksson EL, Wolf-Watz H, Fallman M. 2011. The RACK1 signaling scaffold protein selectively interacts with Yersinia pseudotuberculosis virulence function. PLoS One 6:e16784. https://doi.org/10.1371/journal.pone.0016784.

16. Yang H, Ke Y, Wang J, Tan Y, Myeni SK, Li D, Shi Q, Yan Y, Chen H, Guo Z, Yuan Y, Yang X, Yang R, Du Z. 2011. Insight into bacterial virulence mechanisms against host immune response via the Yersinia pestis-human protein-protein interaction network. Infect Immun 79:4413–4424. https://doi.org/10.1128/IAI.05622-11.

17. Piecha D, Wiberg C, Morgelin M, Reinhardt DP, Deak F, Maurer P, Paulsson M. 2002. Matrilin-2 interacts with itself and with other extracellular matrix proteins. Biochem J 367:715–721. https://doi.org/10.1042/bj20021069.

18. Leong JM, Morrissey PE, Marra A, Isberg RR. 1995. An aspartate residue of the Yersinia pseudotuberculosis invasin protein that is critical for integrin binding. EMBO J 14:422–431.

19. Skrzypek E, Cowan C, Straley SC. 1998. Targeting of the Yersinia pestis YopM protein into HeLa cells and intracellular trafficking to the nucleus. Mol Microbiol 30:1051–1065. https://doi.org/10.1046/j.1365-2958.1998.01135.x.

20. Marketon MM, DePaolo RW, DeBord KL, Jabri B, Schneewind O. 2005. Plague bacteria target immune cells during infection. Science 309:1739–1741. https://doi.org/10.1126/science.1114580.

21. Ramamurthi KS, Schneewind O. 2003. Substrate recognition by the Yersinia type III protein secretion machinery. Mol Microbiol 50:1095–1102. https://doi.org/10.1046/j.1365-2958.2003.03777.x.

22. Whitmore L, Wallace BA. 2004. DICHROWEB, an online server for protein secondary structure analyses from circular dichroism spectroscopic data. Nucleic Acids Res 32:W668–W673. https://doi.org/10.1093/nar/gkh371.

23. Whitmore L, Wallace BA. 2008. Protein secondary structure analyses from circular dichroism spectroscopy: methods and reference databases. Biopolymers 89:392–400. https://doi.org/10.1002/bip.20853.

24. Tsang TM, Felek S, Krukonis ES. 2010. Ail binding to fibronectin facilitates Yersinia pestis binding to host cells and Yop delivery. Infect Immun 78:3358–3368. https://doi.org/10.1128/IAI.00238-10.

25. Felek S, Krukonis ES. 2009. The Yersinia pestis Ail protein mediates binding and Yop delivery to host cells required for plague virulence. Infect Immun 77:825–836. https://doi.org/10.1128/IAI.00913-08.

26. Garcia JT, Ferracci F, Jackson MW, Joseph SS, Pattis I, Plano LR, Fischer W, Plano GV. 2006. Measurement of effector protein injection by type III and type IV secretion systems by using a 13-residue phosphorylatable glycogen synthase kinase tag. Infect Immun 74:5645–5657. https://doi.org/10.1128/IAI.00690-06.

27. Isberg RR, Yang Y, Voorhis DL. 1993. Residues added to the carboxyl terminus of the Yersinia pseudotuberculosis invasin protein interfere with recognition by integrin receptors. J Biol Chem 268:15840–15846.

28. Eitel J, Dersch P. 2002. The YadA protein of Yersinia pseudotuberculosis mediates high-efficiency uptake into human cells under environmental conditions in which invasin is repressed. Infect Immun 70:4880–4891. https://doi.org/10.1128/IAI.70.9.4880-4891.2002.

29. Paerregaard A, Espersen F, Skurnik M. 1991. Role of the Yersinia outer membrane protein YadA in adhesion to rabbit intestinal tissue and rabbit intestinal brush border membrane vesicles. APMIS 99:226–232. https://doi.org/10.1111/j.1699-0463.1991.tb05143.x.

30. Perry RD, Straley SC, Fetherston JD, Rose DJ, Gregor J, Blattner FR. 1998. DNA sequencing and analysis of the low-Ca²⁺-response plasmid pCD1 of Yersinia pestis KIM5. Infect Immun 66:4611–4623.

31. Parkhill J, Wren BW, Thomson NR, Titball RW, Holden MT, Prentice MB, Sebaihia M, James KD, Churcher C, Mungall KL, Baker S, Basham D, Bentley SD, Brooks K, Cerdeno-Tarraga AM, Chillingworth T, Cronin A, Davies RM, Davis P, Dougan G, Feltwell T, Hamlin N, Holroyd S, Jagels K, Karlyshev AV, Leather S, Moule S, Oyston PC, Quail M, Rutherford K, Simmonds M, Skelton J, Stevens K, Whitehead S, Barrell BG. 2001. Genome sequence of Yersinia pestis, the causative agent of plague. Nature 413:523–527. https://doi.org/10.1038/35097083.

32. Miller VL, Beer KB, Heusipp G, Young BM, Wachtel MR. 2001. Identification of regions of Ail required for the invasion and serum resistance phenotypes. Mol Microbiol 41:1053–1062. https://doi.org/10.1046/j.1365-2958.2001.02575.x.

33. Tsang TM, Annis DS, Kronshage M, Fenno JT, Usselman LD, Mosher DF, Krukonis ES. 2012. Ail protein binds ninth type III fibronectin repeat (9FNIII) within central 120-kDa region of fibronectin to facilitate cell binding by Yersinia pestis. J Biol Chem 287:16759–16767. https://doi.org/10.1074/jbc.M112.358978.

34. Payne D, Tatham D, Williamson ED, Titball RW. 1998. The pH 6 antigen of Yersinia pestis binds to beta1-linked galactosyl residues in glycosphingolipids. Infect Immun 66:4545–4548.

35. Galvan EM, Chen H, Schifferli DM. 2007. The Psa fimbriae of Yersinia pestis interact with phosphatidylcholine on alveolar epithelial cells and pulmonary surfactant. Infect Immun 75:1272–1279. https://doi.org/10.1128/IAI.01153-06.

36. Benedek O, Khan AS, Schneider G, Nagy G, Autar R, Pieters RJ, Emody L. 2005. Identification of laminin-binding motifs of Yersinia pestis plasminogen activator by phage display. Int J Med Microbiol 295:87–98. https://doi.org/10.1016/j.ijmm.2005.02.002.

37. Zhang SS, Park CG, Zhang P, Bartra SS, Plano GV, Klena JD, Skurnik M, Hinnebusch BJ, Chen T. 2008. Plasminogen activator Pla of Yersinia pestis utilizes murine DEC-205 (CD205) as a receptor to promote dissemination. J Biol Chem 283:31511–31521. https://doi.org/10.1074/jbc.M804646200.

38. Maldonado-Arocho FJ, Green C, Fisher ML, Paczosa MK, Mecsas J. 2013. Adhesins and host serum factors drive Yop translocation by yersinia into professional phagocytes during animal infection. PLoS Pathog 9:e1003415. https://doi.org/10.1371/journal.ppat.1003415.

39. Achtman M, Zurth K, Morelli G, Torrea G, Guiyoule A, Carniel E. 1999. Yersinia pestis, the cause of plague, is a recently emerged clone of Yersinia pseudotuberculosis. Proc Natl Acad Sci U S A 96:14043–14048. https://doi.org/10.1073/pnas.96.24.14043.

40. Heise T, Dersch P. 2006. Identification of a domain in Yersinia virulence factor YadA that is crucial for extracellular matrix-specific cell adhesion and uptake. Proc Natl Acad Sci U S A 103:3375–3380. https://doi.org/10.1073/pnas.0507749103.

41. Marra A, Isberg RR. 1997. Invasin-dependent and invasin-independent pathways for translocation of Yersinia pseudotuberculosis across the Peyer's patch intestinal epithelium. Infect Immun 65:3412–3421.

42. Fallman M, Gustavsson A. 2005. Cellular mechanisms of bacterial internalization counteracted by Yersinia. Int Rev Cytol 246:135–188. https://doi.org/10.1016/S0074-7696(05)46004-0.

43. Rosqvist R, Skurnik M, Wolf-Watz H. 1988. Increased virulence of Yersinia pseudotuberculosis by two independent mutations. Nature 334:522–524. https://doi.org/10.1038/334522a0.

44. Zhou D, Tong Z, Song Y, Han Y, Pei D, Pang X, Zhai J, Li M, Cui B, Qi Z, Jin L, Dai R, Du Z, Wang J, Guo Z, Wang J, Huang P, Yang R. 2004. Genetics of metabolic variations between Yersinia pestis biovars and the proposal of a new biovar, microtus. J Bacteriol 186:5147–5152. https://doi.org/10.1128/JB.186.15.5147-5152.2004.

45. Yang F, Ke Y, Tan Y, Bi Y, Shi Q, Yang H, Qiu J, Wang X, Guo Z, Ling H, Yang R, Du Z. 2010. Cell membrane is impaired, accompanied by enhanced type III secretion system expression in Yersinia pestis deficient in RovA regulator. PLoS One 5:e12840. https://doi.org/10.1371/journal.pone.0012840.

46. Du Z, Tan Y, Yang H, Qiu J, Qin L, Wang T, Liu H, Bi Y, Song Y, Guo Z, Han Y, Zhou D, Wang X, Yang R. 2009. Gene expression profiling of Yersinia pestis with deletion of lcrG, a known negative regulator for Yop secretion of type III secretion system. Int J Med Microbiol 299:355–366. https://doi.org/10.1016/j.ijmm.2008.10.003.

47. Brown WF. 1964. Variance estimation in the Reed-Muench fifty per cent end-point determination. Am J Hyg (Lond) 79:37–46.

48. Song Y, Tong Z, Wang J, Wang L, Guo Z, Han Y, Zhang J, Pei D, Zhou D, Qin H, Pang X, Zhai J, Li M, Cui B, Qi Z, Jin L, Dai R, Chen F, Li S, Ye C, Du Z, Lin W, Yu J, Yang H, Huang P, Yang R. 2004. Complete genome sequence of Yersinia pestis strain 91001, an isolate avirulent to humans. DNA Res 11:179–197. https://doi.org/10.1093/dnares/11.3.179.